Journal of Materials Chemistry

Cite this: *J. Mater. Chem.*, 2011, **21**, 13247

www.rsc.org/materials

PAPER

High-mobility low-bandgap conjugated copolymers based on indacenodithiophene and thiadiazolo[3,4-*c*]pyridine units for thin film transistor and photovoltaic applications

Ying Sun,[ab] Shang-Chieh Chien,[ac] Hin-Lap Yip,[a] Yong Zhang,[a] Kung-Shih Chen,[a] David F. Zeigler,[d] Fang-Chung Chen,[c] Baoping Lin*[b] and Alex K.-Y. Jen*[a]

Received 12th April 2011, Accepted 30th June 2011
DOI: 10.1039/c1jm11564b

Two new semiconducting polymers based on indacenodithiophene and thiadiazolo[3,4-*c*]pyridine units were synthesized *via* Stille coupling polymerization. The polymers, PIDTPyT and PIDTDTPyT, exhibited main absorption bands in the range of 550–800 nm while their absorption maxima were located at around 700 nm in films. With two additional thiophene spacers, PIDTDTPyT showed a broader absorption band but a 20 nm blue-shifted maximum peak compared to that of PIDTPyT. Both of the polymers possess low bandgaps (~1.6 eV) and deep energy levels for both the highest occupied molecular orbital (HOMO) and the lowest unoccupied molecular orbital (LUMO). Organic field-effect transistors (OFETs) device measurements indicate that PIDTPyT and PIDTDTPyT have high hole carrier mobilities of 0.066 and 0.045 $cm^2\ V^{-1}\ s^{-1}$, respectively, with the on/off ratio on the order of 10^6. Bulk heterojunction photovoltaic devices consisting of the copolymers and $PC_{71}BM$ gave power conversion efficiencies (PCE) as high as 3.91% with broadband photo-response in the range of 300–800 nm. The relationships between the photovoltaic performance and film morphology, energy levels, hole mobilities are discussed.

1. Introduction

Polymer solar cells (PSCs) are considered as one of the most promising alternative to conventional solar cells due to their unique advantages of low cost, light weight, flexibility and processability in large-area substrates.[1–4] So far, the bulk heterojunction (BHJ) structure, which comprises a blend of an electron-rich polymer as donor and an electron-deficient fullerene derivative as acceptor, is the most efficient architecture for PSCs.[5–8] In the past decade, a remarkable amount of efforts to improve the power conversion efficiency (PCE) of PSCs has been devoted to the development of novel conjugated donor polymers.[9–16] It has been demonstrated that the ideal p-type polymer in the BHJ layer should simultaneously possess a strong absorption overlap with the solar spectrum, suitable HOMO–LUMO energy levels to facilitate efficient exciton dissociation in the BHJ while maintaining high open-circuit voltage (V_{oc}), good film morphology and high hole mobility.[2,17–19] Up to now, significant progress has been made for BHJ polymer solar cells with a PCE as high as 7–8%.[7,8]

Recently, indacenodithiophene (IDT) has emerged as a promising donor unit for constructing donor–acceptor (D–A) alternating conjugated copolymers for PSCs.[20–25] The structure is characterized as two thiophene rings rigidified together with a central phenyl ring, which can provide strong intermolecular interactions for ordered packing to improve the charge carrier mobility.[21] Previously, a series of random copolymers based on indacenodithiophene, benzothiadiazole (BT) and thiophene units were synthesized.[24] These polymers showed broad absorption bands, reasonable field-effect hole mobilities (10^{-4} to 10^{-3} $cm^2\ V^{-1}\ s^{-1}$) and promising OPV performance. Recently, Ting *et al.*[23] and Chen *et al.*[22] have reported that an alternating copolymer based on IDT and BT units exhibits a high hole mobility with the PCE over 6%, which is higher than the analogous random copolymers. The PCE of IDT-based polymers can be potentially improved by further deepening the HOMO level to increase the V_{oc} and narrowing the bandgap to enhance light absorption. However, the trade-off between the bandgap and the HOMO–LUMO relationships of the polymer donor and fullerene acceptor makes it difficult to simultaneously optimize the energy levels and bandgap. So further development of new IDT based polymers is very essential to achieve more understanding of the structure–performance relationships.

[a]*Department of Materials Science and Engineering, University of Washington, Seattle, Washington, 98195, USA. E-mail: ajen@u.washington.edu; Fax: +1 206 543 3100; Tel: +1 206 543 2626*
[b]*School of Chemistry and Chemical Engineering, Southeast University, Jiangning District, Nanjing, Jiangsu Province, P.R. China 211189. E-mail: lbp@seu.edu.cn; Fax: +86-25-52090616; Tel: +86-25-52090616*
[c]*Department of Photonics & Display Institute, National Chiao Tung University, Hsinchu, 30010, Taiwan*
[d]*Department of Chemistry, University of Washington, P.O. Box 351700, Seattle, Washington, 98195, USA*

Thiadiazolo[3,4-*c*]pyridine (PyT), which is expected to be a stronger electron acceptor compared to 2,1,3-benzothiadiazole due to the more electron-deficient property of the pyridine, has been less explored in D–A copolymers. Blouin *et al.*[26] incorporated thienyl-flanked PyT with the carbazole unit to yield a low molecular weight copolymer showing limited mobility and efficiency. They demonstrated that the asymmetric structure of the PyT unit may diminish the structural organization of the polymer and consequently decreased the device performance. Recently, a series of polymers copolymerized with various donor moieties and an alkylated thienyl-flanked PyT unit were reported by Zhou *et al.*[27] Encouragingly, these polymers showed good solubility, reduced bandgaps, deeper HOMO–LUMO levels and better performance than their corresponding 1,4-dithien-2-yl-2,1,3-benzothiadiazole (DTBT) based polymers. In spite of the achieved high efficiency based on PyT units, the relationships between the structure, deep energy levels, charge mobility, and device performance still need to be further explored.

To understand these relationships, two new D–A copolymers (PIDTPyT and PIDTDTPyT) were synthesized based on PyT and thienyl-flanked PyT acceptor moieties copolymerized with the IDT donor monomer. After introducing the more electron-deficient PyT unit, both PIDTPyT and PIDTDTPyT showed reduced bandgaps (1.60 eV for PIDTPyT and 1.62 eV for PIDTDTPyT) and deep HOMO energy levels compared to their BT conterparts.[22] OFET measurements showed that the polymers had excellent charge transporting properties with hole mobilities as high as 0.066 $cm^2\ V^{-1}\ s^{-1}$ and an on/off ratio of 10^6. BHJ solar cells based on the blend of the polymers and $PC_{71}BM$ showed the PCEs up to 3.41% and 3.91% for PIDTPyT and PIDTDTPyT, respectively. The main limitation on device performance was the fill factor (FF) though both devices exhibited superior broadband photo-response spectra in the range of 300–800 nm. The small energy offset between the LUMO levels of the polymer and $PC_{71}BM$ as well as the inferior vertical mobility may be the limitation factors for the efficiency.

2. Experimental section

Materials

All chemicals were purchased from Aldrich and TCI without further purification. Diethyl 1,4-bis(thiophen-2-yl)-2,5-benzenedicarboxylate was prepared as reported.[28] Toluene was distilled from sodium and benzophenone ketyl under nitrogen prior to use.

Measurement and characterization

UV-Vis spectra were recorded using a Perkin-Elmer Lambda-9 spectrophotometer. The ^1H NMR and ^{13}C NMR spectra were collected on a Bruker AV 300 or 500 spectrometer operating at 300 or 125 MHz in deuterated chloroform solution with TMS as reference. ESI-MS spectra were recorded on a Bruker APEX Qe 47e Fourier transform (ion cyclotron resonance) mass spectrometer. The molecular weight was measured by a Waters 1515 gel permeation chromatograph (GPC) with a refractive index detector at room temperature (THF as the eluent). Cyclic voltammetries of polymer films were conducted on a BAS CV-50 W voltammetric system with a three-electrode cell in acetonitrile with 0.1 M of tetrabutylammonium hexafluoro-phosphate using a scan rate of 100 mV s^{-1}. ITO, Ag/AgCl and Pt mesh were used as working electrode, reference electrode and counter electrode, respectively. The differential scanning calorimetry (DSC) was performed using a DSC2010 (TA instruments) under a heating rate of 10 °C min^{-1} and a nitrogen flow of 50 mL min^{-1}. The AFM images under tapping mode were taken from the actual devices fabricated for photovoltaic measurement on a Veeco multimode AFM with a Nanoscope III controller.

Synthesis of monomers

Synthesis of compound 1. To a solution of 1-bromo-4-hexylbenzene (3.0 g, 12.5 mmol) in THF (25 mL) was added dropwise *n*-BuLi (5.5 mL, 2.5 M in hexane, 13.75 mmol) at −78 °C. The resulting solution was stirred for 1 h and then quenched with a solution of diethyl 1,4-bis (thiophen-2-yl)-2,5-benzene-dicarboxylate (1.0 g, 2.59 mmol) in THF (15 mL). And the reaction was kept at −78 °C for 1 h, slowly warmed to room temperature and stirred overnight. Water was added to the solution and the mixture was extracted with ethyl acetate. The combined organic layers were dried with Na_2SO_4 and then solvent was removed by rotary evaporation. The resulting white solids were added to acetic acid (30 mL). After the addition of concentrated H_2SO_4 (1 mL), the reaction was allowed to reflux for 5 h and then quenched with water (150 mL). The mixture was extracted with CH_2Cl_2 and the combined organic layer was washed with water for 3 times and dried over Na_2SO_4. Solvent was removed under reduced pressure and the residue was purified by silica gel chromatography (eluent: hexane/dichloromethane = 10/1) to afford a white solid (1.3 g 67%). ^1H NMR ($CDCl_3$, ppm): 7.44 (s, 2H), 7.26 (d, $J = 4.89$ Hz, 2H), 7.15 (d, $J = 8.28$ Hz, 8H), 7.08 (d, $J = 8.31$ Hz, 8H), 7.02 (d, $J = 4.89$ Hz, 2H), 2.57 (t, 8H), 1.58 (m, 4H), 1.31 (m, 28H), 0.88 (t, 12H). ^{13}C NMR ($CDCl_3$, ppm): 156.05, 153.60, 142.27, 141.57, 141.47, 135.30, 128.48, 128.10, 127.59, 123.33, 117.69, 62.85, 35.78, 31.94, 31.57, 29.37, 22.82, 14.32. HRMS (ESI): (M^+, $C_{64}H_{74}S_2$), calcd: 906.5232; found: 906.5201.

Synthesis of compound 2. *n*-BuLi (1.1 mL, 2.5 M in hexane) was added dropwise to a solution of compound **1** (1 g, 1.1 mmol) in THF (20 mL) at −78 °C. The mixture was kept at −78 °C for 30 min and then warmed to room temperature for another 30 min. After cooling to −78 °C again, trimethyltin chloride (2.5 mL, 1 M in hexane) was added. The reaction was stirred overnight at room temperature and then quenched with water, extracted with hexane, and dried over Na_2SO_4. After removal of the solvent, ethanol was added to the mixture and the precipitate was collected as a white solid (1.1 g, 82%). ^1H NMR ($CDCl_3$, ppm): 7.40 (s, 2H), 7.15 (d, $J = 8.04$ Hz, 8H), 7.07 (d, $J = 8.28$ Hz, 8H), 7.03 (s, 2H), 2.56 (t, 8H), 1.58 (m, 4H), 1.31 (m, 28H), 0.89 (t, 12H), 0.35 (s, 18H). ^{13}C NMR ($CDCl_3$, ppm): 157.72, 153.77, 147.55, 142.66, 141.35, 141.15, 134.93, 130.81, 128.39, 128.20, 117.96, 62.33, 35.79, 31.95, 31.55, 29.39, 22.82, 14.32, −7.82. HRMS (ESI): (M^+, $C_{70}H_{90}S_2Sn_2$), calcd: 1234.4528; found: 1234.4480.

Synthesis of compound 3. To a solution of 3,4-diaminopyridine (3.93 g, 36 mmol) in 50 mL 48% aqueous hydrobromic acid was

added slowly 6 mL bromine and the mixture subsequently was allowed to reflux overnight. The mixture was cooled down to room temperature and then filtered. The resultant precipitation was washed sequentially with aq. Na_2CO_3, aq. $Na_2S_2O_3$ and water. The crude product was further refluxed in a 10% solution of Na_2CO_3 for 1 h and then obtained by filtration. Purification by silica gel chromatography (eluent: dichloromethane/ethyl acetate = 10/1) gave **3** (3.5 g, 37%) as a yellow solid. ^{1}H NMR ($CDCl_3$, ppm): 7.89 (s, 1H), 4.49 (s, 2H), 3.68 (s, 2H).

Synthesis of compound 4. To a stirred, cooled solution of 3,4-diamino-2,5-dibromopyridine (1 g, 3.78 mmol) in pyridine (12 mL) at 0 °C was added dropwise $SOCl_2$ (0.4 mL). Stirring was continued for an additional 2 h and then the mixture was poured into water. The crude product was collected by filtration and washed with water. Further purification by silica column chromatography (eluent: hexane/dichloromethane = 4/1) afforded **4** as a pale yellow solid (0.62 g, 56%). ^{1}H NMR ($CDCl_3$, ppm): 8.57 (s, 1H). ^{13}C NMR ($CDCl_3$, ppm): 155.20, 150.22, 145.23, 136.65, 111.68. HRMS (ESI): (M^+, $C_5HN_3SBr_2$) calcd: 292.8258; found: 292.8341.

Synthesis of compound 5. A mixture of compound **3** (0.292 g, 1 mmol) and 2-(tributylstannyl)thiophene (0.970 g, 2.6 mmol) in THF (15 mL) was degassed several times over 1 h. $Pd_2(dba)_3$ (37 mg) and P(*o*-tol)$_3$ (73 mg) were added and the resultant mixture was heated at reflux for 15 h and then allowed to cool. Water was added to the mixture and the aqueous phase was extracted with dichloromethane for three times. The combined organic extracts were dried over Na_2SO_4, filtered and the solvent was removed under vacuum. The crude was further purified with silica column chromatography (eluent: hexane/dichloromethane = 2/1) to give compound **5** as a red solid (0.241 g, 80%). ^{1}H NMR ($CDCl_3$, ppm): 8.88 (s, 1H), 8.74 (dd, J_1 = 3.81 Hz, J_2 = 1.12 Hz, 1H), 8.14 (dd, J_1 = 3.66 Hz, J_2 = 1.1 Hz, 1H), 7.64 (dd, J_1 = 4.80 Hz, J_2 = 1.1 Hz, 1H), 7.52 (dd, J_1 = 5.10 Hz, J_2 = 1.1 Hz, 1H), 7.30 (dd, J_1 = 5.01 Hz, J_2 = 3.8Hz, 1H), 7.27 (dd, J_1 = 4.80 Hz, J_2 = 3.7 Hz, 1H). ^{13}C NMR ($CDCl_3$, ppm): 154.94, 148.03, 146.48, 141.79, 140.80, 136.55, 131.89, 130.54, 128.89, 128.15, 127.87, 127.25, 120.50. HRMS (ESI): (M^+, $C_{13}H_7N_3S_3$) calcd: 300.9802; found: 300.9875.

Synthesis of compound 6. To a solution of compound **4** (0.2 g, 0.664 mmol) in 5 mL chloroform was added the *n*-bromosuccinimide (0.26 g, 1.462 mmol) and the mixture was stirred in the dark for 24 h. The reaction was quenched with water and the water layer was extracted with chloroform. The combined organic layer was dried over Na_2SO_4 and the solvent was removed under vacuum. Purification by the silica column chromatography (eluent: hexane/dichloromethane = 2/1) gave the compound **6** as a dark red solid (0.27 g, 86%). ^{1}H NMR ($CDCl_3$, ppm): 8.73 (s, 1H), 8.43 (d, J = 4.05 Hz, 1H), 7.83 (d, J = 3.99 Hz, 1H), 7.22 (d, J = 4.08 Hz, 1H), 7.18 (d, J = 3.99 Hz, 1H). HRMS (ESI): (M^+, $C_{13}H_5Br_2N_3S_3$) calcd: 456.8012; found: 456.8095.

Synthesis of polymers

Synthesis of polymer PIDTPYT. Compounds **2** (123.4 mg, 0.1 mmol) and **4** (29.3 mg, 0.1 mmol) were charged in a 25 mL flask under N_2 protection. Toluene (4 mL) and DMF (0.4 mL) were added and the mixture was degassed following the quick addition of $Pd_2(dba)_3$ (4 mg) and P(*o*-tol)$_3$ (10 mg). The mixture was heated at reflux for 2 days, cooled to RT and then poured into methanol. The precipitate was collected by filtration and washed by Soxhlet extraction with acetone and hexane for 12 h respectively. Then the resulting solid was dissolved in chloroform and the solution was poured into hexane to afford the polymer PIDTPYT (85 mg, 74%). ^{1}H NMR (500 MHz, $CDCl_3$, δ) 8.80 (br, 1H), 8.63 (br, 1H), 8.10 (br, 1H), 7.57 (dd, 2H), 7.12 (m, 16H), 2.58 (br, 8H), 1.57 (m, 4H), 1.29 (m, 28H), 0.88 (m, 30H). Elemental analysis: calcd C, 79.57; H, 7.16; N, 4.03; found C, 78.81; H, 6.81; N, 3.73%. M_n = 115 kDa, M_w = 267 kDa, PDI = 2.32.

Synthesis of polymer PIDTPYT. Compounds **2** (123.4 mg, 0.1 mmol) and **6** (45.7 mg, 0.1 mmol) were charged in a 25 mL flask under N_2 protection. Toluene (5 mL) and DMF (0.5 mL) were added and the mixture was degassed following the quick addition of $Pd_2(dba)_3$ (4 mg) and P(*o*-tol)$_3$ (10 mg). The mixture was heated at reflux for 2 days, cooled to RT and then poured into methanol. The precipitate was collected by filtration and washed by Soxhlet extraction with acetone and hexane for 12 hours respectively. Then the resulting solid was dissolved in chloroform and the solution was poured into hexane to afford the polymer PIDTDTPYT (67 mg, 56%). ^{1}H NMR (500 MHz, $CDCl_3$, δ) 8.79 (br, 1H), 7.72 (m, 4H), 7.55 (m, 4H), 7.23 (dd, 8H), 7.14 (dd, 8H), 2.60 (br, 8H), 1.70 (m, 4H), 1.37 (m, 28H), 0.92 (m, 30H). Elemental analysis: calcd C, 76.70; H, 6.52; N, 3.48; found C, 75.45; H, 6.16; N, 3.44%. M_n = 32 kDa, M_w = 87 kDa, PDI = 2.73.

Fabrication of the OFET device. The Field-effect transistors were fabricated with a bottom-gate, top-contact configuration. The heavily n-doped silicon substrates with a 300 nm thick thermally grown SiO_2 dielectric (from Montco Silicon Technologies, Inc.) were first cleaned by sonicating in acetone and isopropanol and then exposed to air plasma. The cleaned substrates were then treated with hexamethyldisilazane (HMDS) through vapor phase deposition in a vacuum oven (200 mTorr, 100 °C, 3 h). Subsequently, the semiconductor polymer films were spin-coated in a glove box from their 10 mg mL^{-1} chloroform solutions which were stirred overnight and filtered with a 0.2 μm PTFE filter. Interdigitated source and drain electrodes (L = 1000 μm, W = 12 μm) were deposited by evaporating a 50 nm thick gold film and defined with a shadow mask. The transfer and output characteristics were measured in a glove box using an Agilent 4155B semiconductor parameter analyzer. The saturation field-effect mobility (μ) was calculated from the following equation:

$$I_{ds} = \mu(W/2L)C_i(V_{gs} - V_{th})^2$$

where W and L are the channel width and length, respectively. C_i is the capacitance of the insulating SiO_2 layer per unit area, V_{gs} and V_{th} are the gate voltage and the threshold voltage, respectively. The threshold voltage (V_{th}) was obtained as the x-axis intercept of the linear section of the plot of $(I_{ds})_{1/2}$ *vs.* V_{gs}. The subthreshold swing was estimated by taking the inverse of the slope of I_{ds} *vs.* V_{gs} in the region of exponential current increase.

Fabrication of the photovoltaic and hole only device. To fabricate conventional configuration solar cells, ITO-coated glass substrates (15 Ω sq^{-1}.) were first cleaned with detergent, deionized water, acetone, and isopropyl alcohol. Subsequently, a PEDOT:PSS (Baytron® PVP AI 4083, filtered at 0.45 μm) layer (~45 nm) was spin-coated onto the cleaned ITO-coated glass substrates at 5000 rpm and then annealed at 120 °C for 30 min under ambient conditions. After that, the substrates were loaded into a nitrogen-filled glove-box. Following that, the active layer was spin-coated onto the PEDOT:PSS layer from a homogeneous blending solution of polymer:$PC_{71}BM$. The solution was prepared by dissolving the polymer and $PC_{71}BM$ with a certain blending weight ratio in *o*-dichlorobenzene (*o*-DCB) overnight and filtered with a 0.2 μm PTFE filter. Finally, the substrates were transferred into the evaporator with shadow masks to define the active area of the devices (10.08 mm^2) and pumped under high vacuum (<2 × 10^{-7} Torr). Then calcium (30 nm) and aluminium (100 nm) were thermally evaporated onto the active layer sequentially. The un-encapsulated solar cells were measured in glove box conditions using a Keithley 2400 SMU source measurement unit and an Oriel Xenon lamp (450 W) with an AM1.5 filter as the solar simulator. A reference silicon solar cell with a KG5 filter, which has been previously standardized by the National Renewable Energy Laboratory, was used to calibrate the light intensity to 100 mW cm^{-2}. To fabricate the hole only device, the same procedure as that used for the photovoltaic device was followed except that MoO_3 was used to replace the calcium.

3. Results and discussion

Synthesis part

General synthetic routes of the monomers are described in Scheme 1. The synthesis of compound **1** involved the double addition of the 1-hexylbenzene lithium to the di-ester compound to give the corresponding alcohol, which subsequently underwent an acid-mediated intramolecular cyclization reaction.[28] Lithiation of the compound **1** followed by quenching with trimethyltin chloride afforded the functionalized IDT based monomer **2** in a good yield (82%). Compound **3** was synthesized according to previously reported procedures.[26] The conversion of the compound **3** to the target monomer **4** was conducted through the ring closure reaction with thionyl chloride. To avoid the undesired product with the bromine atom at the 4-position replaced by chlorine atom, pyridine was employed to dissolve the amine compound and absorb the hydrochloric acid. The amount of thionyl chloride was controlled to be around 1.4–1.5 eq. and the reaction was carried out at low temperature. Under these conditions, the pure dibromo functionalized monomer **4** was obtained with a reasonable yield (56%). The purity of the monomer was confirmed by GC-MS and NMR. The Stille coupling reaction between **4** and tributyl (2-thienyl) stannane yielded compound **5** and subsequent bromination by *n*-bromosuccinimide gave the target monomer **6**, which was carefully purified using silica column chromatography.

Scheme 2 depicted the synthetic methods for the polymers. It is worth noting that the polymer structure is regiorandom due to the asymmetric PyT unit. Copolymers PIDTPyT and PIDTDTPyT were then synthesized by Stille cross-coupling reaction of the dibromo monomers (**4** and **6**) with the bis-stannyl compound **2**, using tris(dibenzylidene-acetone)dipalladium(0) (Pd_2dba_3) as catalyst and tri(*o*-tolyl) phosphine ($P(o\text{-tol})_3$) as the corresponding ligand in toluene/DMF solution. The polymerization was taken at 110 °C under nitrogen atmosphere for 48 h. The resulting polymers were collected by directly precipitating the solution in methanol followed by filtration. After Soxhlet extraction with acetone and hexane, the final polymers were further purified by dissolving in $CHCl_3$ and then precipitating in hexane. The two polymers have good solubilities in chlorinated solvents such as chloroform, chlorobenzene and dichlorobenzene. The molecular weights of the two polymers were measured by GPC with polystyrene as standard and THF as eluent. The number-average molecular weight (M_n) of PIDTPyT and PIDTDTPyT is 111.0 kDa and 37.7 kDa, with polydispersity indices (PDI) of 2. 32 and 2.73 (listed in Table 1) respectively. The thermal properties were investigated with differential scanning calorimetry (DSC) but no thermal transition signal was observed in the range from 20 to 350 °C for both of the polymers.

Optical and electrochemical properties

The UV-vis absorption spectra of the two polymers in $CHCl_3$ solutions and films are shown in Fig. 1 and the summarized data are listed in Table 1. Two obvious absorption bands can be observed for the two polymers both in films and solutions. The shorter wavelength absorbance can be assigned to the delocalized π–π* transition in the polymer chains while the absorption band

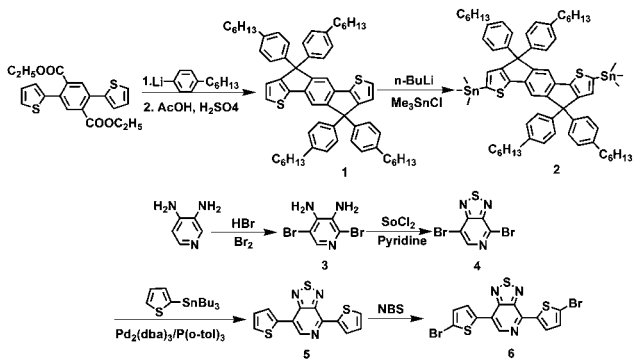

Scheme 1 Synthetic routes for monomers.

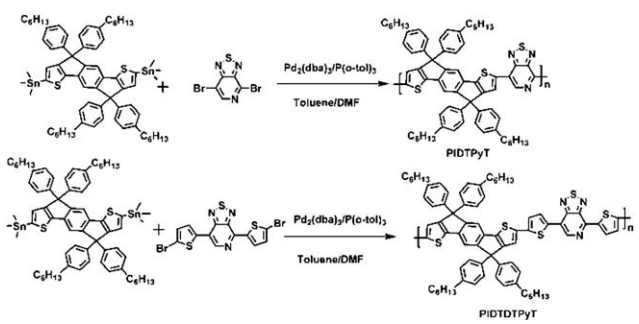

Scheme 2 Synthetic routes for polymers (regiorandom polymer structure).

Table 1 Physical, optical and electrochemical properties of polymers

			UV-vis absorption									
			In $CHCl_3$		In film		Cyclic voltammetry					
Polymer	M_n/kg mol^{-1}[a]	PDI[a]	λ_{max}/nm	λ_{onset}/nm	λ_{max}/nm	λ_{onset}/nm	HOMO/eV	LOMO/eV	Bandgap/eV	Mobility/$cm^2\ V^{-1}\ s^{-1}$	Threshold voltage	On/off ratio
PIDTPyT	111.0	2.32	707	765	707	775	−5.40	−3.80[b]/−3.51[c]	1.60[d]/1.89[c]	0.066[e]/0.062[f]	−18.9[e]/−14.9[f]	10^6
PIDTDTPyT	37.7	2.73	650	745	680	765	−5.32	−3.70[b]/−3.38[c]	1.62[d]/1.94[c]	0.037[e]/0.045[f]	−14.5[e]/−12.4[f]	10^6

[a] Determined from GPC against the polystyrene standard using THF as eluent. [b] Calculated from the optical bandgap and HOMO level. [c] Measured from the cyclic voltammetry. [d] Optical bandgap. [e] As cast. [f] Annealing at 110 °C.

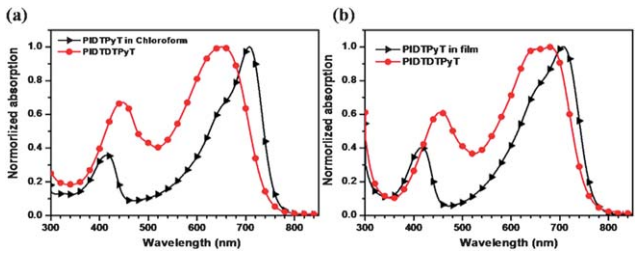

Fig. 1 UV-vis absorption spectra of polymers PIDTPyT and PIDTDTPyT in chloroform solution (a) and in film (b).

in the longer wavelength has been attributed to intramolecular charge transfer (ICT) from the electron-rich IDT units to the electron-deficient PyT functionalities.[2]

The absorption maxima in chloroform solution were observed at 707 and 650 nm for PIDTPyT and PIDTDTPyT, respectively. In the solid state, PIDTPyT showed an absorption spectrum similar to that obtained in the solution with only slightly broader absorption range and a red-shifted (~7 nm) absorption onset. Considering the high molecular weight and the rigid backbone of the polymer, the absence of red-shift in the absorption maxima may originate from the aggregation of the polymer chains formed in solution.[29] The strong internal charge transfer between IDT and PyT would facilitate the polymer backbone to adopt a more planar structure, thereby enhancing the stacking and aggregation of polymer even in solution. The absorption maxima and the onset of PIDTDTPyT were red-shifted from the solution to the solid state with a pronounced shoulder at approximately 680 nm. This indicates a higher structural organization and an ordered packing which may be related to stronger aggregation induced by intermolecular interactions in the solid state.[30]

According to many results published in the literature,[16,31,32] the bandgap of the polymer decreased when extra thiophene units were introduced between the donor and the acceptor due to the more extended and delocalized π-electron system. It is interesting that PIDTDTPyT exhibits a broader absorption range but with blue-shifted absorption maxima and the onset both in solution and in film compared to PIDTPyT. The increased conjugation length can be indicated by the red-shifted short-wavelength absorption band of polymer PIDTDTPyT toward PIDTPyT. However, the magnitude of the red shift in the longer-wavelength absorption band induced by increasing the monomer conjugation length is less pronounced. When more donor units are introduced to the backbone, the concentration of the acceptor units decreases and consequently the accessible ICT decreases to the point where most energy transitions are localized on the donor segments.[33] Therefore, by introducing one thiophene spacer between the donor and the acceptor, the ICT characteristic may be diminished in PIDTDTPyT. Another possible reason may be the less rigid and planar polymer backbone of PIDTDTPyT due to the twist of the polymer chain introduced by the thiophene units, causing reduced conjugation.[34]

Evaluated from the onset of the UV-vis absorption, the bandgaps of the polymers PIDTPyT and PIDTDTPyT were determined to be 1.60 and 1.62 eV, respectively. Compared to the polymer copolymerized with IDT and BT units,[22] PIDTPyT exhibited a bathochromic shift (~60 nm) in the absorption maximum and a reduced optical bandgap (~0.14 eV), which also indicated that the stronger electron-accepting ability of PyT induces more efficient ICT. These low bandgap polymers were expected to give more light absorption and broader photo-response.

Cyclic voltammetry (CV) was employed to evaluate the HOMO and LUMO levels of polymers which were calculated using the following equation:

$$\text{HOMO} = -[E_{ox} + 4.80]\ \text{eV}$$

$$\text{LOMO} = -[E_{red} + 4.80]\ \text{eV}$$

where E_{ox} and E_{red} are the onset of the oxidation and reduction potentials, respectively. The CV curves of polymers are shown in Fig. 2 and the detailed results are listed in Table 1. The HOMO levels of two polymers were found to be −5.40 and −5.32 eV for PIDTPyT and PIDTDTPyT, respectively. The deep HOMO levels may contribute to improve oxidative stability and higher open-circuit voltage (V_{oc}).[35]

The LUMO levels measured by CV were determined to be −3.51 and −3.38 eV for PIDTPyT and PIDTDTPyT, respectively. However, calculated from the HOMO level and the optical bandgap of the polymer films (λ_{onset} of the absorption spectra), the LUMO energy levels were estimated to be −3.80 and −3.70 eV for PIDTPyT and PIDTDTPyT, respectively. The close energetic proximity of the polymer and the LUMO level of $PC_{61}BM$ and $PC_{71}BM$ may diminish the efficient charge separation and lead to increased charge recombination.[36]

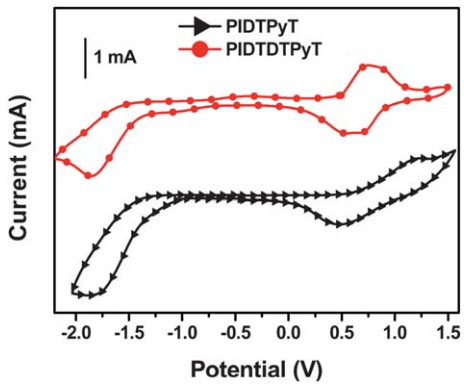

Fig. 2 Cyclic voltammograms of PIDTPyT and PIDTDTPyT (working electrode: ITO; reference electrode: Ag/AgCl; counter electrode: Pt mesh).

To further understand the geometric and electrical properties, density functional theory (DFT) theoretical calculations were performed at the B3LYP/6-31G (d) level by modeling the trimer compounds. Particularly, the hexyl-phenyl side chains were replaced with ethyl–phenyl groups for computational simplicity considering that side-chain substituents have minimal effects on the oxidative and reductive properties of the polymers. The optimized molecular geometries and HOMO and LUMO wave functions are depicted in Fig. 3. For both the polymers, the HOMO wavefunctions are delocalized over the whole conjugated polymer backbone, which indicates that the HOMO levels are determined by both donor and acceptor units. However, the LUMO wave functions for PIDTPyT are primarily localized on PyT units, while they extend onto the thiophene units for PIDTDTPyT. This implies that adding the extra thiophene units has impacts on both the HOMO and LUMO levels. These results from the calculations are in agreement with the experimental values from CV tests. As can be observed, the optimized geometries of the polymers revealed highly planar molecular structures, which can provide more evidence for the planar structure and good packing as previously discussed.

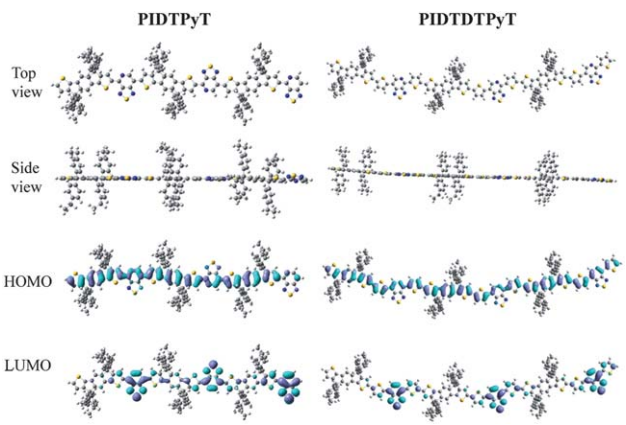

Fig. 3 Molecular geometries and HOMO, LUMO wavefunctions of the trimer model of PIDTPyT and PIDTDTPyT.

Charge transport properties

The charge transport properties of the active materials in BHJ play an important role in the OPV performance. A good carrier mobility ensures efficient exciton dissociation, charge transfer and reduces the charge recombination.[37] Top contact organic field-effect transistor (OFET) devices were fabricated to evaluate the hole mobilities of the polymers. The OFET devices without annealing exhibited the typical p-channel characteristics. Fig. 4 showed the output curves at different gate voltage (V_{gs}) and transfer characteristics in the saturation regime under constant source–drain voltage (V_{ds} = −100 V) for PIDTPyT and PIDTDTPyT. We also investigated the annealing effect on the OFET characteristics and the detailed data including mobilities, on/off ratios, and threshold voltages obtained from the OFETs based on these two polymers before and after annealing are listed in Table 1.

The hole-mobilities of PIDTPyT and PIDTDTPyT without annealing were determined to be 0.066 and 0.037 $cm^2\ V^{-1}\ s^{-1}$, respectively, with the on/off ratio at the order of 10^6. After annealing at 110 °C, the mobility of PIDTPyT remained essentially constant while PIDTDTPyT showed an increased mobility of 0.045 $cm^2\ V^{-1}\ s^{-1}$. The high charge mobility indicates that there are strong intermolecular interactions induced by the aforementioned π–π stacking and donor–acceptor interactions. The fused ring aromatic structure of the IDT unit may generate better molecular organization and provide highly efficient pathways for charge carrier transport. PyT may help promote the donor–acceptor interaction and decrease the intramolecular stacking distance.[36] The negligible annealing effect on the mobility for PIDTPyT also indicated this strong intermolecular interaction of polymer chains. The lower mobility of PIDTDTPyT may be ascribed to weaker intermolecular interactions due to the additional thiophene

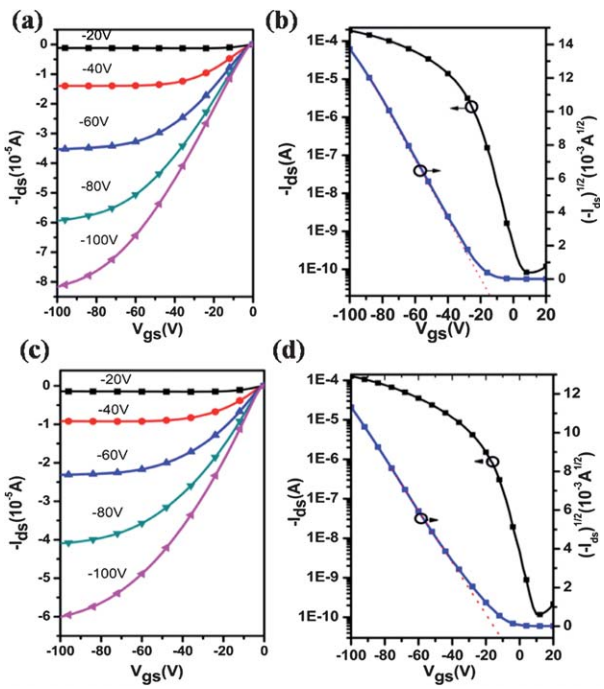

Fig. 4 Output (a and c) and transfer (b and d) characteristics of PIDTPyT (a and b) and PIDTDTPyT (c and d).

spacers. And the interaction can be enhanced upon annealing, therefore promoting polymer chains form more ordered organization in film to result in higher mobility.

Photovoltaic properties

The photovoltaic properties of PIDTPyT and PIDTDTPyT were investigated with the conventional device structure of ITO/PEDOT:PSS(40 nm)/polymer:$PC_{71}BM$/Ca(30 nm)/Al(100 nm), where the device area is 10.08 mm^2. $PC_{71}BM$, which features a wider absorption region compared to $PC_{61}BM$, was chosen as the n-type acceptor in order to efficiently utilize the solar light. The BHJ active layer was prepared by spin-coating dichlorobenzene solution of the polymer:$PC_{71}BM$ on a PEDOT:PSS layer. All the devices were annealed in 150 °C for 15 min before the electrode deposition. The variation effects of the blending ratio, which seriously influence the charge balance characteristics and consequently determine the device performance, were investigated in detail. The summarized electrical parameters of these OPV devices are listed in Table 2. Higher current density (J_{sc}), FF and the resulting PCE were obtained under the ratio of 1 : 3, which may be due to the optimized electron–hole charge balance and reduced charge recombination.

Photovoltaic devices based on PIDTPyT:$PC_{71}BM$ (1 : 3) with the optimized thickness of 68 nm showed a PCE value up to 3.41% with a J_{sc} of 10.03 mA cm^{-2}, a V_{oc} of 0.82 V, and a FF of 42%. For PIDTDTPyT-based devices, a highest resulting PCE of 3.91% with the optimized thickness of 80 nm was achieved when the FF improved to 50%, and the J_{sc} and V_{oc} decreased slightly to 9.89 mA cm^{-2} and 0.79 V compared to PIDTPyT. Representative *J–V* curves of these two devices measured under illumination (100 mA cm^{-2}, AM 1.5G) are plotted in Fig. 5(a) based on the optimized conditions. Notably, the active layer thickness of the devices is only around 60–80 nm corresponding to the photocurrent of *ca.* 10 mA cm^{-2}, indicating that the two polymers blended with $PC_{71}BM$ featured good absorption properties. Moreover, Fig. 5(b) displays the external quantum efficiency (EQE) and UV-vis spectra of the two polymers and $PC_{71}BM$. The EQE spectra were tightly correlated with the UV-vis absorption of the bulk heterojunctions. Compared to PIDTDTPyT, the EQE curve for PIDTPyT exhibited weaker photoresponse between 350 and 610 nm but increased EQE between 610 and 800 nm, which can be explained by the more red-shifted absorption of PIDTPyT. To conclude, both devices based on these two low-bandgap materials blended with $PC_{71}BM$ exhibited superior broadband photo-response spectra covering 300–800 nm. The limitation to the better performance was the poor fill factor which has been found to be related to the film morphology, charge transfer and the recombination process.[1,3,18]

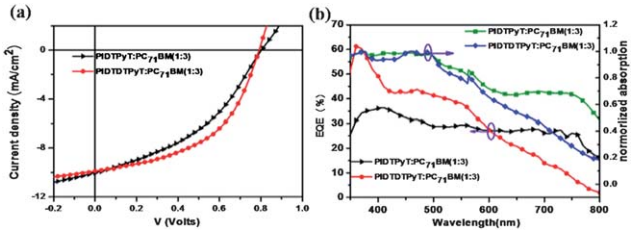

Fig. 5 Current–voltage characteristics (a) and EQE wavelength dependencies (b) of photovoltaic devices based on PIDTPyT and PIDTDTPyT with the blending ratio as 1:3 under illumination with 100 mW cm^{-2} (AM 1.5G).

Optimal phase segregation and formation of a bicontinuous interpenetrating network between the polymer donor and PCBM acceptor are critical to achieve high device performance and largely influence the charge separation and exciton dissocation.[38–40] Tapping-mode atomic force microscopy (AFM) was used to investigate the morphology of thin films of the BHJ blends of the polymer and $PC_{71}BM$. As shown in Fig. 6, the BHJ films showed very smooth surfaces with the rms roughness around ~0.5 nm and no obvious large-scale phase separation was observed. This indicated that both polymers have good film-forming abilities and compatibilities with $PC_{71}BM$.

Additionally, the difference in the LUMO energy level between the acceptor and donor is one another of the critical factors determining the exciton dissociation rate and charge recombination.[18,41] From prior discussion on device performance, the FF is the main limitation on device performance. We speculate that a certain degree of electron–hole recombination would occur in these blending systems, thereby lowering the FF. From the energy level point of view, the LUMO levels of PIDTPyT and PIDTDTPyT are respectively −3.80 eV and −3.70 eV, which may be too close to the LUMO level of $PC_{71}BM$ (−4.3 eV). Thus, the exciton may not efficiently dissociate into

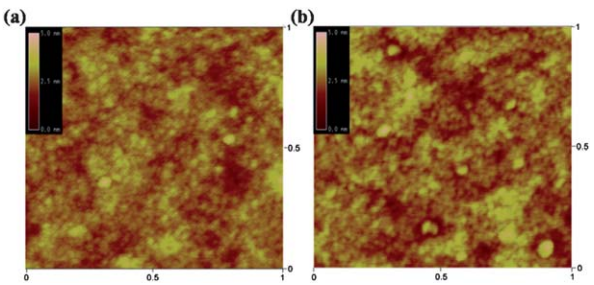

Fig. 6 AFM images (1 μm × 1 μm) for the films of polymer:$PC_{71}BM$ (1 : 3): (a) PIDTPyT and (b) PIDTDTPyT as cast from *o*-DCB solutions.

Table 2 Summarized performances of devices containing PIDTPyT and PIDTDTPyT with different polymer:$PC_{71}BM$ blending ratios

Polymer	Blend ratio	V_{oc}/v	J_{sc}/mA cm^{-2}	FF (%)	PCE (%)
PIDTPyT	1 : 2	0.80	8.86	39	2.73
	1 : 3	0.82	10.03	42	3.41
	1 : 4	0.76	9.35	40	2.87
PIDTDTPyT	1 : 2	0.77	8.88	44	3.03
	1 : 3	0.79	9.89	50	3.91
	1 : 4	0.62	3.65	45	1.03

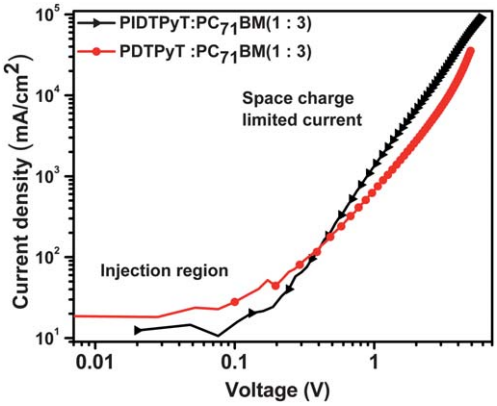

Fig. 7 Current density and voltage (J–V) curves of the hole-only devices containing polymer and $PC_{71}BM$ with the ratio of 1 : 3. ($V = V_{applied} - V_{bi}$, $V_{bi} = 0.1$ V).

separated free charges and the charge recombination rate may potentially increase. The higher FF obtained from PIDTDTPyT based devices might be correlated with its higher LUMO level compared to the PIDTPyT-based device.

Although the results based on a field-effect transistor indicated that both PIDTPyT and PIDTDTPyT feature superior lateral hole carrier-transport abilities, the vertical hole carrier-transport behaviours of the polymers blended with the fullerene play an essential role in the photovoltaic devices performance.[42] Herein, hole-only devices based on ITO/PEDOT:PSS/BHJ/MoO_3/Al were fabricated to measure the vertical hole mobility. MoO_3 was used as an interfacial layer to suppress electron injection from Al so that the hole-only current was measured.[43] Fig. 7 shows the current density and voltage curve (J–V) of the hole-only devices containing polymer and $PC_{71}BM$ with the blending ratio of 1 : 3. The space charge limited current (SCLC) model was employed to investigate the vertical hole mobilities using the following equation, $J = 9\varepsilon_0\varepsilon_r\mu V^2/8L^3$, where J is the current density (mA cm^{-2}), $\varepsilon_0\varepsilon_r$ is the permittivity of the polymer, μ is the carrier mobility, and L is the active layer thickness. The mobilities were extracted by modelling the dark current in the SCLC region. The calculated vertical hole-transport mobilities of PIDTPyT and PIDTDTPyT are 6.34×10^{-5} and 7.97×10^{-5} (cm^2 V^{-1} s^{-1}), respectively, which are lower than the FET mobilities by three orders of magnitude. This discrepancy indicates that the vertical hole-transporting ability was greatly inferior to the lateral mobility, which might cause charge recombination issues, thereby leading to lower FF and thinner optimized device thickness.[41]

4. Conclusion

To conclude, we have synthesized two new low bandgap polymers (PIDTPyT and PIDTDTPyT) through the Stille polymerization between the IDT donor and PyT as well as thienyl-flanked PyT acceptor monomers. The stronger acceptor character of the PyT unit broadened the absorption spectrum of the polymers to longer wavelengths and resulted in deep energy levels. The OFET results showed that the two polymers have high lateral hole mobilities as high as 0.066 cm^2 V^{-1} s^{-1}. However, the vertical mobilities of the polymers as measured by the SCLC method were determined as three orders of magnitude lower than the FET mobilities. The photovoltaic properties of the polymers were investigated and the highest achieved PCEs for PIDTPyT and PIDTDTPyT were 3.41% and 3.91%, respectively. The deep LUMO level of the polymers combined with the low vertical mobilities may not allow efficient charge dissociation and separation, which may give rise to the limitation on photovoltaic performance.

Acknowledgements

This work is supported by the National Science Foundation's NSF-STC program under Grant No. DMR-0120967, the AFOSR (FA9550-09-1-0426), the Office of Naval Research (N00014-11-1-0300), and the World Class University (WCU) program through the National Research Foundation of Korea under the Ministry of Education, Science and Technology (R31-21410035). A.K.-Y.J. thanks the Boeing-Johnson Foundation for financial support. Y. Sun thanks the State-Sponsored Scholarship for Graduate Students from China Scholarship Council. S. C. Chien thanks the National Science Council of Taiwan (NSC98-2917-I-009-112) for supporting the Graduate Students Study Abroad Program.

Notes and references

1 S. Gunes, H. Neugebauer and N. S. Sariciftci, *Chem. Rev.*, 2007, **107**, 1324.
2 Y. J. Cheng, S. H. Yang and C. S. Hsu, *Chem. Rev.*, 2009, **109**, 5868.
3 G. Dennler, M. C. Scharber and C. J. Brabec, *Adv. Mater.*, 2009, **21**, 1323.
4 J. Y. Kim, K. Lee, N. E. Coates, D. Moses, T. Q. Nguyen, M. Dante and A. J. Heeger, *Science*, 2007, **317**, 222.
5 G. Yu, J. Gao, J. C. Hummelen, F. Wudl and A. J. Heeger, *Science*, 1995, **270**, 1789.
6 M. C. Scharber, D. Wuhlbacher, M. Koppe, P. Denk, C. Waldauf, A. J. Heeger and C. L. Brabec, *Adv. Mater.*, 2006, **18**, 789.
7 H. Y. Chen, J. H. Hou, S. Q. Zhang, Y. Y. Liang, G. W. Yang, Y. Yang, L. P. Yu, Y. Wu and G. Li, *Nat. Photonics*, 2009, **3**, 649.
8 Y. Y. Liang, Z. Xu, J. B. Xia, S. T. Tsai, Y. Wu, G. Li, C. Ray and L. P. Yu, *Adv. Mater.*, 2010, **22**, E135.
9 J. W. Chen and Y. Cao, *Acc. Chem. Res.*, 2009, **42**, 1709.
10 Y. Y. Liang, D. Q. Feng, Y. Wu, S. T. Tsai, G. Li, C. Ray and L. P. Yu, *J. Am. Chem. Soc.*, 2009, **131**, 7792.
11 J. H. Hou, H. Y. Chen, S. Q. Zhang, R. I. Chen, Y. Yang, Y. Wu and G. Li, *J. Am. Chem. Soc.*, 2009, **131**, 15586.
12 F. Huang, K. S. Chen, H. L. Yip, S. K. Hau, O. Acton, Y. Zhang, J. D. Luo and A. K. Y. Jen, *J. Am. Chem. Soc.*, 2009, **131**, 13886.
13 Y. P. Zou, A. Najari, P. Berrouard, S. Beaupre, B. R. Aich, Y. Tao and M. Leclerc, *J. Am. Chem. Soc.*, 2010, **132**, 5330.
14 Y. Zhang, S. K. Hau, H. L. Yip, Y. Sun, O. Acton and A. K. Y. Jen, *Chem. Mater.*, 2010, **22**, 2696.
15 J. Peet, J. Y. Kim, N. E. Coates, W. L. Ma, D. Moses, A. J. Heeger and G. C. Bazan, *Nat. Mater.*, 2007, **6**, 497.
16 J.-Y. Wang, S. K. Hau, H.-L. Yip, J. A. Davies, K.-S. Chen, Y. Zhang, Y. Sun and A. K. Y. Jen, *Chem. Mater.*, 2010, **23**, 765.
17 B. C. Thompson and J. M. J. Frechet, *Angew. Chem., Int. Ed.*, 2008, **47**, 58.
18 T. M. Clarke and J. R. Durrant, *Chem. Rev.*, 2010, **110**, 6736.
19 P.-L. T. Boudreault, A. Najari and M. Leclerc, *Chem. Mater.*, 2010, **23**, 456.
20 Y. Zhang, J. Zou, H.-L. Yip, K.-S. Chen, D. F. Zeigler, Y. Sun and A. K. Y. Jen, *Chem. Mater.*, 2011, **23**, 2289.
21 W. M. Zhang, J. Smith, S. E. Watkins, R. Gysel, M. McGehee, A. Salleo, J. Kirkpatrick, S. Ashraf, T. Anthopoulos, M. Heeney and I. McCulloch, *J. Am. Chem. Soc.*, 2010, **132**, 11437.
22 K. S. Chen, Y. Zhang, H. L. Yip, Y. Sun, J. A. Davies, C. Ting, C. P. Chen and A. K. Y. Jen, *Org. Electron.*, 2011, **12**, 794.

23 Y. C. Chen, C. Y. Yu, Y. L. Fan, L. I. Hung, C. P. Chen and C. Ting, *Chem. Commun.*, 2010, **46**, 6503.
24 C. P. Chen, S. H. Chan, T. C. Chao, C. Ting and B. T. Ko, *J. Am. Chem. Soc.*, 2008, **130**, 12828.
25 C. Y. Yu, C. P. Chen, S. H. Chan, G. W. Hwang and C. Ting, *Chem. Mater.*, 2009, **21**, 3262.
26 N. Blouin, A. Michaud, D. Gendron, S. Wakim, E. Blair, R. Neagu-Plesu, M. Belletete, G. Durocher, Y. Tao and M. Leclerc, *J. Am. Chem. Soc.*, 2008, **130**, 732.
27 H. X. Zhou, L. Q. Yang, S. C. Price, K. J. Knight and W. You, *Angew. Chem., Int. Ed.*, 2010, **49**, 7992.
28 K. T. Wong, T. C. Chao, L. C. Chi, Y. Y. Chu, A. Balaiah, S. F. Chiu, Y. H. Liu and Y. Wang, *Org. Lett.*, 2006, **8**, 5033.
29 E. G. Wang, L. T. Hou, Z. Q. Wang, S. Hellstrom, F. L. Zhang, O. Inganas and M. R. Andersson, *Adv. Mater.*, 2010, **22**, 5240.
30 M. M. Wienk, M. Turbiez, J. Gilot and R. A. J. Janssen, *Adv. Mater.*, 2008, **20**, 2556.
31 K. C. Li, J. H. Huang, Y. C. Hsu, P. J. Huang, C. W. Chu, J. T. Lin, K. C. Ho, K. H. Wei and H. C. Lin, *Macromolecules*, 2009, **42**, 3681.
32 W. Y. Wong, X. Z. Wang, Z. He, K. K. Chan, A. B. Djurisic, K. Y. Cheung, C. T. Yip, A. M. C. Ng, Y. Y. Xi, C. S. K. Mak and W. K. Chan, *J. Am. Chem. Soc.*, 2007, **129**, 14372.
33 P. M. Beaujuge, C. M. Amb and J. R. Reynolds, *Acc. Chem. Res.*, 2010, **43**, 1396.
34 J. C. Bijleveld, M. Shahid, J. Gilot, M. M. Wienk and R. A. J. Janssen, *Adv. Funct. Mater.*, 2009, **19**, 3262.
35 L. J. Huo, J. H. Hou, S. Q. Zhang, H. Y. Chen and Y. Yang, *Angew. Chem., Int. Ed.*, 2010, **49**, 1500.
36 D. Muhlbacher, M. Scharber, M. Morana, Z. G. Zhu, D. Waller, R. Gaudiana and C. Brabec, *Adv. Mater.*, 2006, **18**, 2884.
37 Z. Zhu, D. Waller, R. Gaudiana, M. Morana, D. Muhlbacher, M. Scharber and C. Brabec, *Macromolecules*, 2007, **40**, 1981.
38 H. Hoppe and N. S. Sariciftci, *J. Mater. Chem.*, 2006, **16**, 45.
39 X. N. Yang, J. Loos, S. C. Veenstra, W. J. H. Verhees, M. M. Wienk, J. M. Kroon, M. A. J. Michels and R. A. J. Janssen, *Nano Lett.*, 2005, **5**, 579.
40 W. L. Ma, C. Y. Yang, X. Gong, K. Lee and A. J. Heeger, *Adv. Funct. Mater.*, 2005, **15**, 1617.
41 M. Lenes, M. Morana, C. J. Brabec and P. W. M. Blom, *Adv. Funct. Mater.*, 2009, **19**, 1106.
42 H. Xin, G. Q. Ren, F. S. Kim and S. A. Jenekhe, *Chem. Mater.*, 2008, **20**, 6199.
43 V. Shrotriya, Y. Yao, G. Li and Y. Yang, *Appl. Phys. Lett.*, 2006, **89**, 063505.